Connected Slot Array with Interchangeable ADL Radome for sub-8 GHz 5G Applications

Ozzola, Riccardo; Neto, Andrea; Imberg, Ulrik; Cavallo, Daniele

DOI
10.1109/TAP.2023.3333541

Publication date
2024

Document Version
Final published version

Published in
IEEE Transactions on Antennas and Propagation

Communication

Connected Slot Array With Interchangeable ADL Radome for Sub-8 GHz 5G Applications

Riccardo Ozzola, Andrea Neto, Ulrik Imberg, and Daniele Cavallo

***Abstract*— We present a dual-polarized connected array of slots with an artificial dielectric layer (ADL) radome for mobile communication applications operating in the sub-6 GHz and the upper 6 GHz bands of 5G. The radiating slots are combined with two interchangeable ADL radomes with different thicknesses, targeting the bands 6–8 and 2–8 GHz, respectively. This highlights the main property of the ADL radome, which realizes an impedance transformer whose bandwidth is proportional to the height of the structure. Moreover, the ADL anisotropy allows for wide scanning, up to 60° in the main planes for both radomes, without scan blindness. An 8 × 8 prototype array has been manufactured and tested with the two ADL radomes. The measured results of the active voltage standing wave ratio (VSWR) and the radiation patterns are reported to validate the design.**

***Index Terms*— 5G antenna arrays, artificial dielectrics, connected arrays, mobile communications, phased arrays, wideband (WB) arrays.**

I. Introduction

The fifth-generation (5G) communication standard exploits massive multiple input multiple output (MIMO) to achieve high data rate streams [1], [2], [3]. With this paradigm, directive beams are radiated toward the different users and steered over a wide field of view to track the user's movements. This motivates the need for wide-scanning arrays to cover the entire field of view with a limited number of antenna panels (e.g., three panels with a scan range of ±60°).

Moreover, 5G relies on the possibility of transmitting information over different frequency ranges of the electromagnetic spectrum. Several bands are already in use between 2 and 6 GHz, and one more band located between 6.425 and 7.125 GHz, i.e., the upper 6 GHz (U6G) band [4], will be licensed in a few years. Resonant antennas are currently being employed on base stations. However, due to their narrowband (NB) properties, multiple antenna arrays are needed to transmit over all the required bands, leading to several radiators competing for the same space or increasing the overall space occupied by the base station. For this reason, wideband (WB) arrays that can operate simultaneously over multiple bands with a single aperture are gaining interest for 5G applications both for the sub-6 GHz band [5], [6], and for the millimeter wave frequencies [7], [8], [9]. Although WB arrays are characterized by a high inter-element mutual coupling, they can still operate in an MIMO environment by generating independent beams, as recently discussed in [10], [11], and [12].

Manuscript received 4 July 2023; revised 27 October 2023; accepted 11 November 2023. Date of publication 22 November 2023; date of current version 9 February 2024. This work was supported by HUAWEI Technologies Sweden AB, UNB Project, under Grant YBN2020045031. *(Corresponding author: Riccardo Ozzola.)*

Riccardo Ozzola, Andrea Neto, and Daniele Cavallo are with the Microelectronics Department of the Electrical Engineering, Mathematics and Computer Science Faculty, Delft University of Technology, 2628 CD Delft, The Netherlands (e-mail: R.Ozzola-1@tudelft.nl).

Ulrik Imberg is with Huawei Technologies Sweden AB, 164 40 Kista, Sweden.

Color versions of one or more figures in this communication are available at https://doi.org/10.1109/TAP.2023.3333541.

Digital Object Identifier 10.1109/TAP.2023.3333541

The past decade has witnessed great advances in the development of phased arrays with WB and wide-scanning capability. Several solutions have been proposed in the literature, including tapered slot antennas [13], [14], [15], metal flared-notch elements [16], [17], long-slot arrays [18], [19], and tightly-coupled or connected dipole arrays [20], [21], [22], [23], [24]. Despite the significant advance of WB phased arrays, the main target applications of these antennas have been defense radars, satellite communications, and radio astronomy. Their use for commercial wireless communications has been hindered by the high complexity and the high cost typically involved in the manufacturing of WB arrays. Most of these arrays are realized with vertically oriented printed circuit boards (PCBs), which are difficult to assemble and unsuitable for mass production. Planar solutions based on a single multi-layer PCB have been proposed to reduce the complexity for tightly coupled dipoles in [25] and [26], and more recently for connected slots in the presence of artificial dielectric layers (ADLs) in [27] and [28]. This latter exploits ADL superstrates, consisting of layers made of sub-wavelength square metal patches, which synthesize an equivalent anisotropic medium [29]. The advantages of an ADL superstrate can be summarized as follows.

1) It diverts a large fraction of the power radiated by the slots towards the upper medium, allowing to reduce the distance from the ground plane so that standard through-hole via technology can be used to realize the feeding lines.
2) It acts as a WB impedance transformer between the free space and the feed impedance of the slots.
3) It increases the scan range by suppressing the surface waves.

In this work, we present the design of an array based on the connected slot element with ADL superstrate, as shown in Fig. 1(a) for the simplified single-pol unit cell. The focus of this design is to show the flexibility of the concept using the same connected array with different ADL radomes to select its operational bandwidth, as shown in Fig. 1(b). In this way, a single antenna section can be used for different applications and environments. As the ADL acts as an impedance transformer, the array impedance bandwidth is strongly related to the ADL design and can be enlarged by increasing the number of metal layers and the overall height of the ADL stackup. More specifically, two ADLs designs are presented, one operating from 6 to 8 GHz, referred to as NB, and the other operating from 2 to 8 GHz, indicated as WB. In both cases, the array can scan up to 60° in both main planes within the frequency bands mentioned above. Furthermore, the WB ADL radome presented here improves the bandwidth of this concept with respect to previous designs [27], [28], by targeting two octaves. Finally, an 8 × 8 dual polarized prototype array is realized, and the resulting measurements are presented with both NB and WB radomes.

II. Unit Cell Design

A. ADL Synthesis

The first step of the unit cell design involves the synthesis of the ADLs to realize a two- and four-section Chebyshev impedance

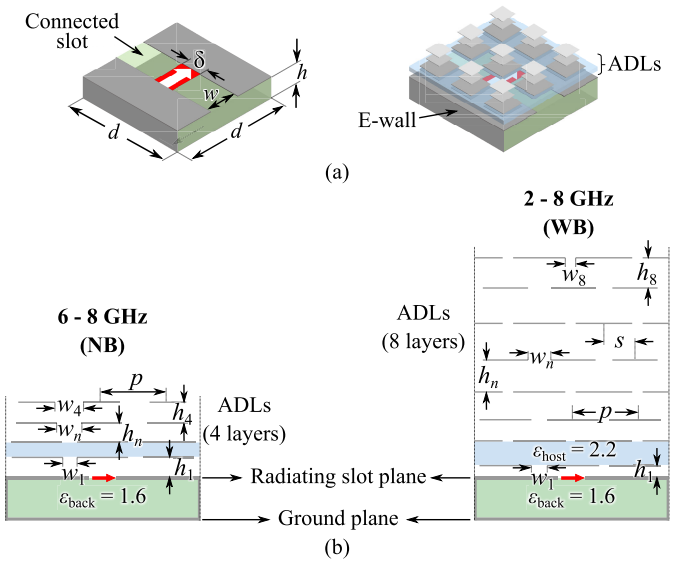

Fig. 1. (a) Sketch of the single polarized connected unit cell without and with the ADL radome. (b) Side view of the array consisting of the common radiating section and the interchangeable ADLs radomes.

TABLE I
GEOMETRICAL PARAMETERS OF THE NB ADL RADOME IN MM

h_1	h_2	h_3	h_4	w_1	w_2	w_3	w_4
0.64	1.53	2.50	3.48	0.50	0.53	1.31	1.3

TABLE II
GEOMETRICAL PARAMETERS OF THE WB ADL RADOME IN MM

h_1	h_2	h_3	h_4	h_5	h_6	h_7	h_8
0.5	2.24	2.95	3.40	3.65	4.90	5.79	6.67
w_1	w_2	w_3	w_4	w_5	w_6	w_7	w_8
0.35	0.18	0.33	0.17	0.63	0.63	1.76	1.76

transformer for the NB and WB, respectively. The impedance transformers, aimed at matching the feeding line of the array element to free space, are initially modeled as a cascade of multiple quarter-wave sections of ideal transmission lines. Each transmission line section can be represented as a homogeneous and isotropic dielectric slab as if a single plane wave were impinging from broadside. Then, each slab is replaced with ADLs having, for normal incidence, the same effective refractive index of the corresponding homogeneous dielectric [30], [31], using the ADL closed-form description derived in [32]. For the case at hand, this results in a transformer made of four and eight layers of patches for the NB and WB case, respectively.

In the ADLs radome design, we introduce a dielectric slab of relative permittivity $\varepsilon_{\text{host}} = 2.2$ between the first two bottom layers. In this way, we obtain a less varying effective permittivity with respect to the scan angle for transverse magnetic (TM) waves and in turn, a more stable active impedance when scanning in the E-plane. The thin dielectric can also be seen as a wide-angle impedance matching layer as originally introduced in [33].

Both of the synthesized ADL radomes have a period $p = 5$ mm, and the other geometrical parameters defined in Fig. 1(b) have the values listed in Tables I and II for the NB and the WB ADL, respectively. The parameter s indicates the shift between odd and even layers in the ADL stack. No inter-layer shift is applied in the NB ADL radome, i.e., the gaps between patches in different layers are vertically aligned. On the contrary, the maximum shift $s = p/2$ has

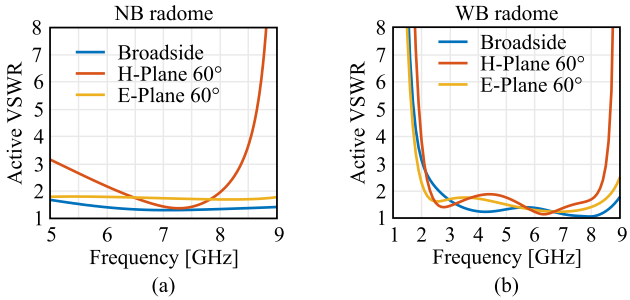

Fig. 2. Active VSWR of the single polarized unit cell for broadside, H-Plane 60° and E-plane 60° scanning. (a) NB ADL. (b) WB ADL radome.

been used for all the metal layers of the WB ADL, resulting in a glide symmetric structure that is characterized by a larger effective permittivity [29].

B. Single-Pol Unit Cell

The single-polarized (single-pol) connected slot unit cell is sketched in Fig. 1(a), and it is designed in the presence of the ADL using the analytical procedure illustrated in [27]. To enhance the bandwidth, the period is set to $d = 0.4\lambda_0^{8\,\text{GHz}} = 15$ mm, and vertical walls have been added between parallel slots (E-walls) to avoid the propagation of guided modes in the substrate below the slots [27]. The slot has a width $w = 0.1\lambda_0^{8\,\text{GHz}}$, it is fed by a δ-gap generator with length $\delta = 0.24\lambda_0^{8\,\text{GHz}}$, and it is separated from the ground plane by a dielectric with thickness $h = 3.5$ mm and relative permittivity $\varepsilon_{\text{back}} = 1.6$.

The corresponding active voltage standing wave ratio (VSWR) is shown in Fig. 2. For the NB radome, the active VSWR is <2.2 when scanning up to 60° on the main planes over the frequency bands of interest, i.e., 6–8 GHz. For the WB radome, a VSWR < 2 is obtained when scanning up to 60° on the main planes over most of the 2–8 GHz frequency band, with an increase to VSWR $= 3$ at the low end of the band (2 GHz).

C. Dual-Pol Unit Cell

Using CST Microwave Studio, the dual-polarized (dual-pol) unit cell sketched in Fig. 3 is designed. This comprises two sets of orthogonal 45° tapered slots, each excited by a microstrip below the array plane, as shown in Fig. 3(a). The feeding microstrip is terminated with a capacitive plate that compensates for the inductive effect of the ground plane. The microstrip is connected with an integrated coaxial line that goes through the holed ground plane to the outer SMP connector, as shown in Fig. 3(b). The integrated coaxial line also has the role of suppressing modes that would otherwise propagate between the ground plane and the slot plane [27]. The specific design for the integrated coaxial feed and for the microstrip transition to the SMP connector is reported in [34]. To avoid the excitation of waves guided by the slot when scanning in the H-plane, the dielectric used to sustain the array plane has been milled into a grid to obtain a lower effective permittivity. The detailed stackups of the array and radomes boards used for the prototyping are shown in Figs. 3(c) and 4, respectively. The ADL geometry has been slightly adjusted to account for the effect of the realistic materials on the layers' reactance.

The simulated active VSWR is shown in Fig. 5 for the NB and WB case, respectively. The VSWR of the NB case is lower than 2 for broadside and E-plane scanning to 60° over the 6–8 GHz range, while it increases to 2.3 when scanning in the H-plane to 60° at 8 GHz. For the WB radome, the simulations show a VSWR < 3 in

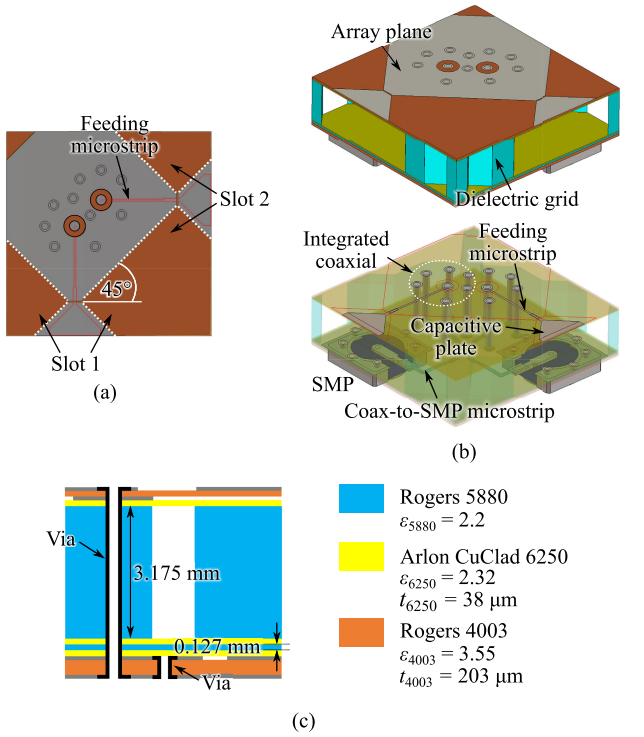

Fig. 3. Sketch of the dual polarized unit cell. (a) Top view. (b) Three-dimensional view, highlighting the array plane, the feeding components, and the dielectric grid. (c) Side view of the stackup.

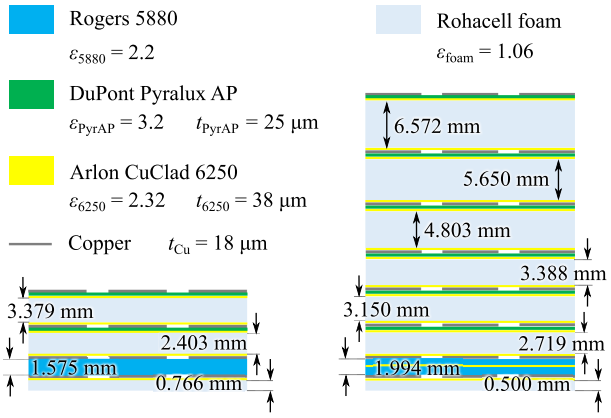

Fig. 4. Stackup of the prototyped NB and WB ADL radomes.

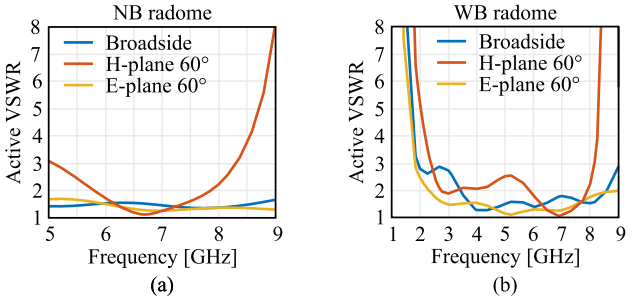

Fig. 5. Active VSWR of the dual polarized unit cell for broadside, H-plane 60°, and E-plane 60° scanning. (a) NB ADL. (b) WB ADL radome.

the 2–8 GHz band for broadside and E-plane scanning, while the bandwidth is reduced to 2.3–8 GHz when scanning to the maximum angle in the H-plane.

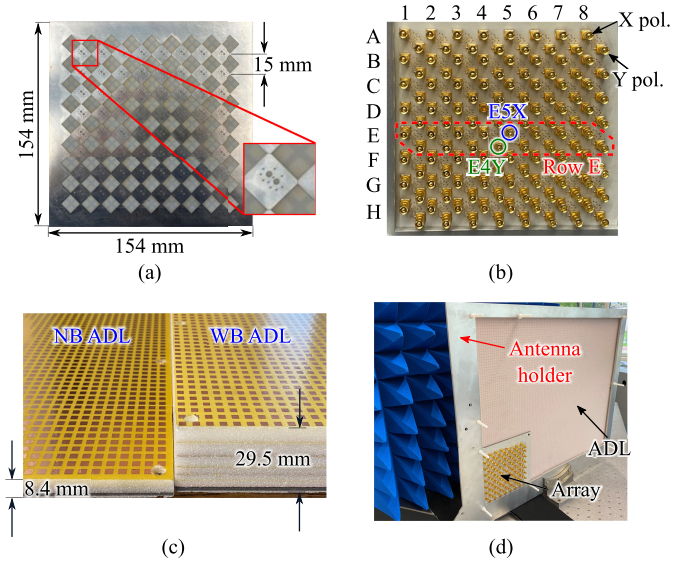

Fig. 6. (a) Front and (b) back view of the manufactured 8 × 8 dual polarized connected slot array prototype. (c) Photograph of the NB and WB ADL radomes. (d) Full setup with array prototype, the NB ADL radome, and the holder.

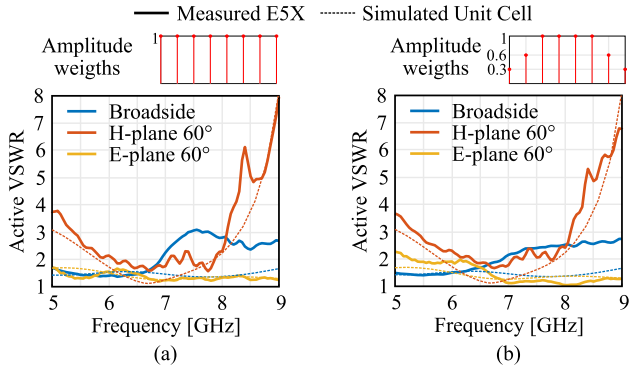

Fig. 7. Measured active VSWR of E5X, when using the NB ADL radome, for broadside, H-Plane 60°, and E-plane 60° scanning. (a) Fully excited array. (b) Array with a tapered excitation.

III. Connected Array Prototype

An 8 × 8 array, based on the dual-polarized unit cell of Fig. 3, has been manufactured [see Fig. 6(a) and (b)] as a representative prototype. The two manufactured ADL radome boards are shown in Fig. 6(c) and have a total thickness of 8.4 and 29.5 mm for the NB and WB, respectively. The antenna is mounted in a holder with the NB or the WB ADL radome, as shown in Fig. 6(d). The radomes are larger than the slot array, as they are intended to be used also for larger antenna arrays or multiple tiles.

A. Measured Active Matching

All the S-parameters between the elements E5X and E4Y [see Fig. 6(b)] and the rest of the array are measured for the NB and WB case, respectively. Then, these are combined with complex weights corresponding to the different scanning and taper conditions, to obtain the active reflection coefficient and VSWR.

The active VSWR of E5X with the NB radome is shown in Fig. 7 for broadside, and scanning to 60° in the main planes. As can be noticed, the fully excited array of Fig. 7(a) has a good agreement with the simulated unit cell results when scanning in the main planes. The measured active VSWR for broadside is slightly higher than the unit cell simulation for frequencies above 7 GHz. This can be partly

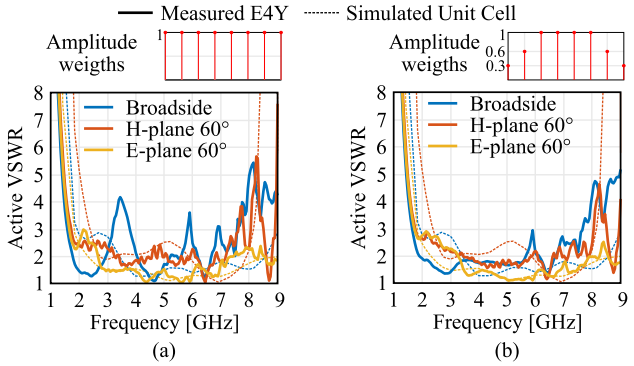

Fig. 8. Measured active VSWR of E4Y, when using the WB ADL radome, for broadside, H-Plane 60°, and E-plane 60° scanning. (a) Fully excited array. (b) Array with a tapered excitation.

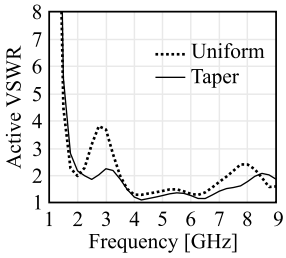

Fig. 9. Simulated active VSWR of a central element in the $8 \times \infty$ configuration for a uniform illumination and an amplitude taper.

attributed to finite edge effects, as an amplitude taper applied to both rows and columns is shown to lower the VSWR below 2.5 on the band of interest, as shown in Fig. 7(b).

The measured active VSWR of the element E4Y with the WB radome is shown in Fig. 8, for different scanning and illumination conditions. The strong mismatch at 3.5 GHz in Fig. 8(a) is due to the resonant size of the full array. In fact, the tapered excitation of Fig. 8(b) effectively removes the resonance. Even in the presence of the amplitude taper, some fast oscillations are seen at around 6 GHz and above. These were observed to be caused by a somewhat unstable connection of the coaxial cables with the smooth bore SMP connectors that gave some variability of the S-parameters depending on the specific position in which the cables were held. Nevertheless, as shown in Fig. 8(b), when applying an amplitude taper, the VSWR of the element E4Y is <3 in the band from 1.7 to 7.6 GHz, corresponding to a 4.5:1 bandwidth.

To verify that the peak at 3.5 GHz is due to the edge effects, an $8 \times \infty$ array simulation has been performed: Fig. 9 shows the active VSWR of a central element, exhibiting a resonance around 3 GHz, which is mitigated when introducing an amplitude taper.

B. Measured Patterns

When operating with either radomes, the E- and H-plane embedded element patterns (EEPs) have been measured for all the elements of both polarizations located in row E [see Fig. 6(b)]. To compensate for the manufacturing tolerances and errors introduced by the measurement setup, the amplitudes and phases of the EEPs are adjusted to compensate for the variations in the broadside direction (i.e., a broadside calibration). Then, the desired array patterns are calculated and shown in Figs. 10 and 11 for the NB and WB case, respectively. The patterns of the uniformly illuminated array are shown at 7 GHz for the NB case and at 2, 5, and 7.5 GHz for the WB case and compared with $8 \times \infty$ CST simulations. A good

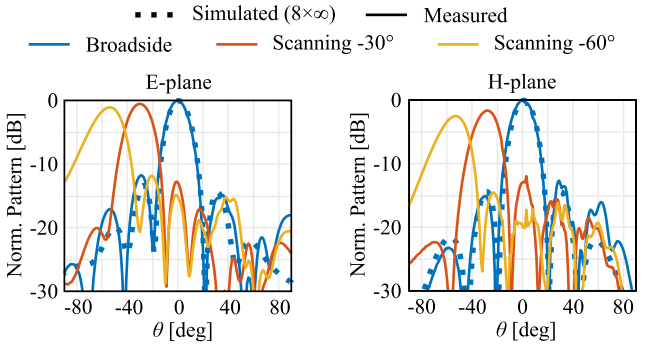

Fig. 10. Measured and simulated ($8 \times \infty$) array patterns on the E-plane and on the H-plane at 7 GHz in the presence of the NB ADL radome.

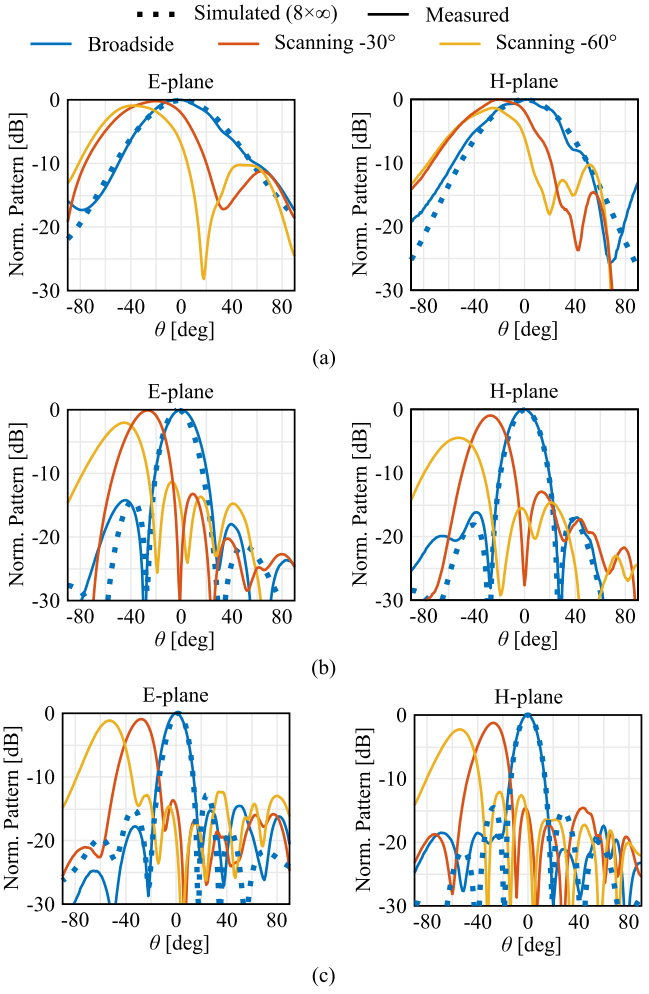

Fig. 11. Measured and simulated ($8 \times \infty$) array patterns in the E-plane and in the H-plane at (a) 2 GHz, (b) 5 GHz, and (c) 7.5 GHz in the presence of the WB ADL radome.

agreement can be recognized for the main lobes and the sidelobe level (SLL), while the discrepancies for larger observation angles are credited to the diffraction from the metal frame. The scanning array patterns are normalized with respect to the broadside values. As it can be noticed, the E- and the H-plane have different scan loss. This difference is mainly due to the different shapes of the EEP in the two planes. The EEPs of the elements in the central row are presented in Fig. 12, showing a larger decay for the H-plane. Moreover, when scanning in the H-plane, a slightly higher mismatch occurs with respect to the E-plane. Due to edge effects, oscillations

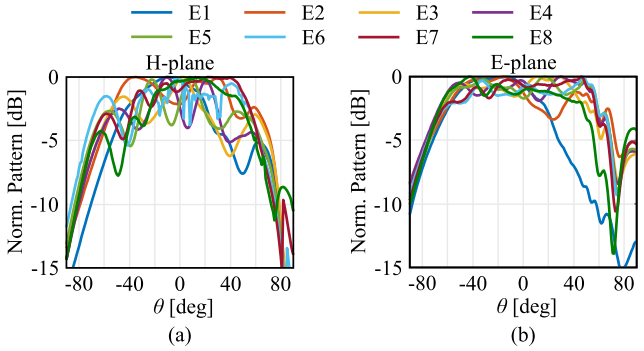

Fig. 12. Measured on (a) H-plane and (b) E-plane at 7 GHz in the presence of the NB ADL radome.

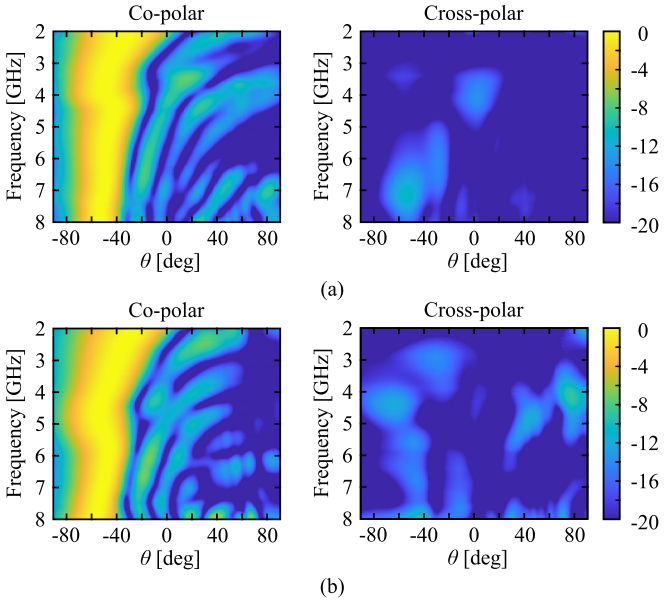

Fig. 13. Measured co-polar and cross-polar component when scanning towards 60° on (a) E-plane and (b) H-plane with the WB radome.

are present in the EEPs, larger in the H-plane compared to the E-plane. Nevertheless, these fluctuations average out when the EEPs are combined together, creating smooth array patterns. Moreover, the diffraction from the metal frame supporting the antenna is visible, especially in the E-plane for large angles.

Radiators in the presence of ADLs exhibit increased cross-polarization levels, especially in the diagonal plane (D-plane). However, in the desired application the scanning in azimuth is much larger than in elevation, e.g., ±20° in the urban scenario of [35], reducing the scanning requirements in the D-plane. In Fig. 13 the co- and cross-polar are shown when scanning towards 60° on the E- and H-plane, exhibiting between 2 and 7.6 GHz a rejection better than −10 and −12 dB, respectively.

IV. Conclusion

A dual-polarized planar connected slot array has been designed to target sub-8 GHz 5G applications. The same radiating aperture is used with two interchangeable ADL radomes, one for 6–8 GHz operation and the other for 2–8 GHz.

An 8 × 8 connected array prototype has been manufactured and tested for impedance and radiation characteristics. When using a tapered illumination, this shows a VSWR < 2.5 when scanning up to 60° with the NB ADL radome over the targeted band and a VSWR < 3 when scanning up to 60° with the WB ADL radome between 1.7 and 7.6 GHz.

Acknowledgment

The authors would like to thank Zhuang Chen for his help in the feed design and to Juan Bueno and Pascal Aubry for their support in the measurements.

References

[1] E. G. Larsson, O. Edfors, F. Tufvesson, and T. L. Marzetta, "Massive MIMO for next generation wireless systems," *IEEE Commun. Mag.*, vol. 52, no. 2, pp. 186–195, Feb. 2014.

[2] E. Bjornson, L. van der Perre, S. Buzzi, and E. G. Larsson, "Massive MIMO in sub-6 GHz and mmWave: Physical, practical, and use-case differences," *IEEE Wireless Commun.*, vol. 26, no. 2, pp. 100–108, Apr. 2019.

[3] W. Hong et al., "Multibeam antenna technologies for 5G wireless communications," *IEEE Trans. Antennas Propag.*, vol. 65, no. 12, pp. 6231–6249, Dec. 2017.

[4] *Radio-Frequency Channel Arrangements for Medium- and High-Capacity Digital Fixed Wireless Systems Operating in the 6425–7125 MHz Band*, document ITU-R F.384-11, Int. Telecommun. Union, Geneva, Switzerland, 2012. [Online]. Available: https://www.itu.int/rec/R-REC-F.384-11-201203-I

[5] Y. Wang, L. Zhu, H. Wang, Y. Luo, and G. Yang, "A compact, scanning tightly coupled dipole array with parasitic strips for next-generation wireless applications," *IEEE Antennas Wireless Propag. Lett.*, vol. 17, no. 4, pp. 534–537, Apr. 2018.

[6] D.-M. Sun, Z.-C. Hao, W.-Y. Liu, and C.-Y. Ding, "An ultrawideband dual-polarized phased array antenna for sub-3-GHz 5G applications with a high polarization isolation," *IEEE Trans. Antennas Propag.*, vol. 71, no. 5, pp. 4055–4065, May 2023.

[7] M. H. Novak, F. A. Miranda, and J. L. Volakis, "Ultra-wideband phased array for millimeter-wave ISM and 5G bands, realized in PCB," *IEEE Trans. Antennas Propag.*, vol. 66, no. 12, pp. 6930–6938, Dec. 2018.

[8] S. M. Moghaddam, J. Yang, and A. U. Zaman, "Fully-planar ultra-wideband tightly-coupled array (FPU-TCA) with integrated feed for wide-scanning millimeter-wave applications," *IEEE Trans. Antennas Propag.*, vol. 68, no. 9, pp. 6591–6601, Sep. 2020.

[9] T.-L. Zhang, L. Chen, S. M. Moghaddam, A. U. Zaman, and J. Yang, "Millimeter-wave ultrawideband circularly polarized planar array antenna using bold-C spiral elements with concept of tightly coupled array," *IEEE Trans. Antennas Propag.*, vol. 69, no. 4, pp. 2013–2022, Apr. 2021.

[10] I. Tzanidis et al., "Method and apparatus for miniaturization of MIMO systems via tightly coupled antenna array," U.S. Patent 0 334 565 A1, Nov. 2014.

[11] R. Ozzola, D. Cavallo, and A. Neto, "On the relation between beam coupling and feed coupling in wideband antenna arrays," *IEEE Trans. Antennas Propag.*, vol. 70, no. 1, pp. 260–267, Jan. 2022.

[12] M. Akrout, V. Shyianov, F. Bellili, A. Mezghani, and R. W. Heath, "Super-wideband massive MIMO," *IEEE J. Sel. Areas Commun.*, vol. 41, no. 8, pp. 2414–2430, Aug. 2023, doi: 10.1109/JSAC.2023.3288269.

[13] D. H. Schaubert, S. Kasturi, A. O. Boryssenko, and W. M. Elsallal, "Vivaldi antenna arrays for wide bandwidth and electronic scanning," in *Proc. 2nd Eur. Conf. Antennas Propag., EuCAP*, Edinburgh, U.K., Nov. 2007, pp. 1–6.

[14] J. J. Lee, S. Livingston, and R. Koenig, "A low-profile wide-band (5:1) dual-pol array," *IEEE Antennas Wireless Propag. Lett.*, vol. 2, pp. 46–49, 2003.

[15] W. Elsallal et al., "Charateristics of decade-bandwidth, Balanced Antipodal Vivaldi Antenna (BAVA) phased arrays with time-delay beamformer systems," in *Proc. IEEE Int. Symp. Phased Array Syst. Technol.*, Waltham, MA, USA, Oct. 2013, pp. 111–116.

[16] H. Holter, "Dual-polarized broadband array antenna with BOR-elements, mechanical design and measurements," *IEEE Trans. Antennas Propag.*, vol. 55, no. 2, pp. 305–312, Feb. 2007.

[17] R. W. Kindt and W. R. Pickles, "Ultrawideband all-metal flared-notch array radiator," *IEEE Trans. Antennas Propag.*, vol. 58, no. 11, pp. 3568–3575, Nov. 2010.

[18] J. J. Lee, S. Livingston, R. Koenig, D. Nagata, and L. L. Lai, "Compact light weight UHF arrays using long slot apertures," *IEEE Trans. Antennas Propag.*, vol. 54, no. 7, pp. 2009–2015, Jul. 2006.

[19] J. J. Lee, S. Livingston, and D. Nagata, "A low profile 10:1 (200–2000 MHz) wide band long slot array," in *Proc. IEEE Antennas Propag. Soc. Int. Symp.*, San Diego, CA, USA, Jul. 2008, p. 14.

[20] J. P. Doane, K. Sertel, and J. L. Volakis, "A wideband, wide scanning tightly coupled dipole array with integrated balun (TCDA-IB)," *IEEE Trans. Antennas Propag.*, vol. 61, no. 9, pp. 4538–4548, Sep. 2013.

[21] W. F. Moulder, K. Sertel, and J. L. Volakis, "Ultrawideband superstrate-enhanced substrate-loaded array with integrated feed," *IEEE Trans. Antennas Propag.*, vol. 61, no. 11, pp. 5802–5807, Nov. 2013.

[22] M. H. Novak and J. L. Volakis, "Ultrawideband antennas for multiband satellite communications at UHF-Ku frequencies," *IEEE Trans. Antennas Propag.*, vol. 63, no. 4, pp. 1334–1341, Apr. 2015.

[23] R. J. Bolt et al., "Characterization of a dual-polarized connected-dipole array for Ku-band mobile terminals," *IEEE Trans. Antennas Propag.*, vol. 64, no. 2, pp. 591–598, Feb. 2016.

[24] D. Cavallo, A. Neto, G. Gerini, A. Micco, and V. Galdi, "A 3− to 5-GHz wideband array of connected dipoles with low cross polarization and wide-scan capability," *IEEE Trans. Antennas Propag.*, vol. 61, no. 3, pp. 1148–1154, Mar. 2013.

[25] S. S. Holland, D. H. Schaubert, and M. N. Vouvakis, "A 7–21 GHz dual-polarized planar ultrawideband modular antenna (PUMA) array," *IEEE Trans. Antennas Propag.*, vol. 60, no. 10, pp. 4589–4600, Oct. 2012.

[26] J. A. Kasemodel, C.-C. Chen, and J. L. Volakis, "Wideband planar array with integrated feed and matching network for wide-angle scanning," *IEEE Trans. Antennas Propag.*, vol. 61, no. 9, pp. 4528–4537, Sep. 2013.

[27] W. H. Syed, D. Cavallo, H. T. Shivamurthy, and A. Neto, "Wideband, wide-scan planar array of connected slots loaded with artificial dielectric superstrates," *IEEE Trans. Antennas Propag.*, vol. 64, no. 2, pp. 543–553, Feb. 2016.

[28] D. Cavallo, W. H. Syed, and A. Neto, "Connected-slot array with artificial dielectrics: A 6 to 15 GHz dual-pol wide-scan prototype," *IEEE Trans. Antennas Propag.*, vol. 66, no. 6, pp. 3201–3206, Jun. 2018.

[29] D. Cavallo and C. Felita, "Analytical formulas for artificial dielectrics with nonaligned layers," *IEEE Trans. Antennas Propag.*, vol. 65, no. 10, pp. 5303–5311, Oct. 2017.

[30] A. Van Katwijk and D. Cavallo, "Analysis and design of connected slot arrays with artificial dielectrics," in *Proc. IEEE Int. Symp. Phased Array Syst. Technol. (PAST)*, Waltham, MA, USA, Oct. 2019, pp. 1–5.

[31] A. J. V. Katwijk, A. Neto, G. Toso, and D. Cavallo, "Design of wideband wide-scanning dual-polarized phased array covering simultaneously both the Ku- and the Ka-satcom bands," in *Proc. 14th Eur. Conf. Antennas Propag. (EuCAP)*, Copenhagen, Denmark, Mar. 2020, pp. 1–3.

[32] D. Cavallo and R. M. van Schelven, "Closed-form analysis of artificial dielectric layers with non-periodic characteristics," in *Proc. 13th Eur. Conf. Antennas Propag. (EuCAP)*, Warsaw, Poland, Mar. 2019, pp. 1–5.

[33] E. Magill and H. Wheeler, "Wide-angle impedance matching of a planar array antenna by a dielectric sheet," *IEEE Trans. Antennas Propag.*, vol. AP-14, no. 1, pp. 49–53, Jan. 1966.

[34] Z. Chen, "Wideband feeding network design for dual-polarized connected arrays," M.S. thesis, Fac. EEMCS, Delft Univ. Technol., Delft, The Netherlands, 2021. [Online]. Available: http://resolver.tudelft.nl/uuid:bb021e79-fcd5-42c4-a9ee-b91855f3af63

[35] J. Fuhl, J.-P. Rossi, and E. Bonek, "High-resolution 3-D direction-of-arrival determination for urban mobile radio," *IEEE Trans. Antennas Propag.*, vol. 45, no. 4, pp. 672–682, Apr. 1997.